Technical Article

Application of Ultrafine Bubbles to Grinding Processes

HATAYAMA Yousuke・MIZUTANI Masayoshi

Abstract

Ultrafine bubbles (UFBs) are microbubbles with diameters below 1 μm. Recent studies have shown that using a coolant containing UFBs (UFB coolant) in grinding processes can improve grinding performance and machining accuracy. However, the mechanism behind this effect remains unclear. While some studies attribute the improved performance to the superior wettability of UFB coolant compared to conventional coolant, this alone cannot fully explain the effects, as there are instances where UFB coolant does not provide significant benefits.

One notable property of UFBs is their ability to generate hydroxyl radicals (OH) upon collapse, which may promote oxidation on workpiece surfaces. This study explores the role of surface oxidation in the grinding performance of UFB coolant. Experiments revealed that the degree of surface oxidation and the composition of oxides vary depending on the type of gas used in UFB water. Friction and wear tests further demonstrated that the gas type in UFB coolant affects the coefficient of friction, which aligns with differences in grinding performance. These findings suggest that the oxidation induced by UFBs influences the friction and wear characteristics of workpieces, leading to changes in grinding performance.

1 Introduction

The term "fine bubbles" is a general term for microbubbles having a diameter of 100 μ m or below. Bubbles with diameters above 1 μ m are called microbubbles, and those having a diameter of 1 μ m or below are called ultrafine bubbles (UFBs). This terminology is defined by the International Organization for Standardization (ISO) [1].

One characteristic of UFBs is that they are colorless and transparent. They also remain in water for a long time. Due to these characteristics, UFBs are used in various fields such as cleaning, disinfection, and water purification [2]. In recent years, many studies [3-8] have reported that the use of coolant containing UFBs (UFB coolant) in grinding processes can improve grinding performance and machining accuracy. In these studies, the reasons for this effect have been investigated and discussed mainly from the point of view of wettability. Kobayashi et. al. reported that UFB coolant contributes to lower contact angle than conventional coolant [6], while Watanabe et. al. reported that UFB coolant contributes to lower slip angle and lower surface tension than conventional coolant [7][8].

On the other hand, we have indicated that there is no significant difference in wettability between conventional coolant and UFB coolant depending on the presence or absence of UFBs and have confirmed that the grinding performance varies even in this situation [9]. This result suggests that the effect of UFBs in grinding processes may involve a factor other than wettability. We think that this factor is due to the collapse of UFBs.

It is known that when UFBs collapse, their interiors reach high temperatures and high pressures due to adiabatic compression and that collapsing UFBs break the surrounding water particles to generate hydroxyl (HO) radicals [Note 1], which are strong oxidants [10][11], and release high-pressure energy to the surrounding substances. Focusing on these phenomena, we have also confirmed that, when a piece of carbon steel is immersed in refined water or UFB water, stronger oxidation of the workpiece surface occurs in the UFB water. Additionally, we have confirmed that

there is a difference in the friction characteristics of the oxidants generated on the workpiece surface depending on the presence or absence of UFBs [9].

In light of the above findings, this paper investigates and discusses how UFBs may affect grinding processes from the point of view of workpiece surface oxidation. Specifically, we hypothesized that the degree of workpiece surface oxidation can vary with the type of UFB gas, as long as the probability of UFB collapse depends on the type of UFB gas and the UFB collapse affects the workpiece. Based on this hypothesis, we immersed test pieces in several UFB waters with different types of gas and UFB coolant and left them as they were to observe changes in surface properties. We then examined changes in the composition of the oxidants produced and the effect of these changes on the friction and wear characteristics of the materials. In addition, assuming actual machining, we immersed untreated test pieces (not previously immersed or left in UFB water or UFB coolant) in UFB coolant and subjected them to friction and wear tests to determine their changes. Finally, we performed a surface grinding test using a common grinder to validate the hypothesis.

Note 1) Highly reactive chemical species composed of oxygen and hydrogen atoms. Have strong power to cause oxidation reaction.

2 Experimental Methods

2. 1 UFB Generation Conditions

In this paper, a UFB generator originally developed by KYB [9][12] was used. Of the various UFB generation principles [13], the rotary shear method with a static mixer was chosen for the generator to achieve high density and high flow rate. Four evaluation fluids were used: [1] purified water, [2] UFB water, [3] coolant diluted with purified or tap water, and [4] UFB coolant. The coolant used was a water-soluble synthetic solution type with a concentration of 2.5%. Fluid [2] was purified water exposed to the UFB generator. Fluid [3] was the coolant that had been diluted to a specified concentration with purified water for immersion or friction/wear testing, or with tap water for grinding testing, and then circulated (mixed) in the UFB generator without gas injection. Fluid [4] was the same coolant as [3] that was introduced into the UFB generator and subjected to gas injection to generate UFBs. Table 1 shows the UFB generation conditions, where the gas concentration is the ratio of the gas flow rate to the fluid flow rate (volumetric flow rate at standard conditions), and the number of passes is the number of times the fluid was circulated. The number of passes for UFB generation was set as shown in Table 1 for the following reasons. The number of passes for water was set at 360 to achieve a UFB number concentration of approximately 1.0 billion/mL. The number of passes for coolant was set at 40, which has been shown to improve the

grinding ratio [9]. Three gases were selected for the following reasons. Air was chosen because of its widespread use and high practicality. O_2 was chosen because we believed that an O_2-rich environment was suitable for aggressive oxidation of the workpiece. CO_2 was chosen because existing studies had shown that the CO_2-UFB density decreased by 90% 30 minutes after UFB generation, causing CO_2-UFBs to collapse easily [14]. When UFBs collapse, OH radicals are generated [10][11] to facilitate oxidation of the workpiece.

The initial UFB number concentration of UFB water was 1.14 billion/mL for Air-UFB, 0.96 billion/mL for O_2-UFB, and 0.11 billion/mL for CO_2-UFB. CO_2-UFB generation was only about one-tenth that of the other gases, even under the same generation conditions. This is probably because CO_2-UFBs collapse easily in the stage immediately following UFB generation and are unable to remain stable bubbles for long.

Several methods exist for measuring UFB number concentration [15]. In this paper, particle tracking analysis (NanoSight NS300 NTA3.4, Malvern) was employed. In this method, particles suspended in a liquid are illuminated with a laser to emit scattered light, which is captured by an objective lens and filmed. This allows all particles to be tracked on the screen, allowing particle size and number to be measured from their Brownian motion velocity [16]. However, it should be noted that this method could not quantify the number of UFBs in the UFB coolant, because the method cannot distinguish UFBs from particles in the coolant itself, due to the measurement principle.

Table 1 UFB generation conditions

Liquid	Type	Water	Coolant
Gas	Type	Air, O_2, CO_2	
	Concentration	2.5%	
Disk speed		2400rpm	
Number of passes		360	40

2. 2 Test pieces

The test pieces used in this paper were made of S50C (or S45C according to a component analysis from the corrosion rate and XPS mentioned later), which had been quenched and tempered to have a hardness of 504.1 to 591.3 HV (N = 10 measurements). Their dimensions were 50 mm (length) x 50 mm (width) x 10 mm (thickness). One test piece was cut into 15 mm x 15 mm pieces for use in the immersion or friction/wear test. The surface of the test piece to be evaluated in the immersion or friction/wear test had been ground prior to use to remove any cutting marks or oxidation scale. The surface roughness after grinding was R_a 0.36 to 0.48 μm (N = 10 measurements).

2.3 Immersion Test

To determine the effects of the UFB collapse and gas type on the oxidation of the test piece surface,

the test piece was immersed in the evaluation fluids. Changes in the test piece were visually observed. Fig. 1 shows a sketch of the immersion test. 400 mL of evaluation fluid was poured into a glass bottle, and the test piece was immersed with the surface to be evaluated facing up and left standing. The test piece surface was visually inspected for five days. If the surface was oxidized, the oxides were evaluated for composition and corrosion rate.

The composition of the oxides was analyzed by X-ray spectroscopy (XPS) [Note 2) 17)]. An XPS analyzer (Thete Probe, Thermo Scientific) was used for the composition analysis.

Corrosion rate is a measure of how much a metal corrodes over a given period of time. We evaluated the corrosion rate to determine how deep the oxidation was progressing. In general, the corrosion rate is determined based on the decrease in mass of the test piece because some types of corrosion can progress locally, making it difficult to determine the decrease in thickness of the test piece. The corrosion rate can be calculated using the following equation [18)]:

$$W = \frac{M_1 - M_2}{S \times T} \tag{1}$$

where W is the corrosion rate [mdd], M_1 is the mass of the test piece before the test [mg], M_2 is the mass of the test piece after the test [mg], S is the surface area of the test piece [dm^2], and T is the number of days of the test. A higher corrosion rate indicates a higher degree of corrosion. In this paper, the corrosion rate was evaluated three days after the immersion.

Note 2)A method of qualitatively analyzing elements on the surface of a material, or analyzing the chemical composition and chemical bonding state of the surface, by detecting and measuring the spectrum of light electrons emitted by samples of the material when irradiated with X-rays.
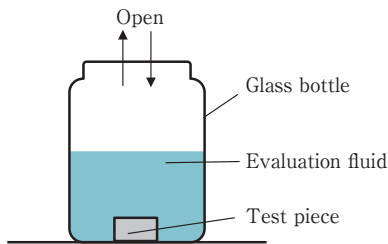

Fig. 1 Sketch of immersion test

2. 4 Evaluation of Friction and Wear Characteristics

Assuming the use of UFBs in grinding processes, friction and wear tests were conducted to clarify the phenomena of friction and wear between the workpiece and the abrasive grains. A ball-on-disk type testing machine was used for these tests. Fig. 2 shows the experimental system. A friction and wear testing machine (FPR-2000, RHESCA) was used in the experiments. As shown in the figure, the test piece is mounted on a tray fixed on a table. The table is moved linearly from side to side to slide the test piece against the ball. The ball is then pulled in the sliding direction due to the friction force between the ball and the test piece. This friction force is measured by a load cell inside the tester and divided by the weight of the load (applied load) to obtain the coefficient of friction. The ball is made of aluminum oxide, which corresponds to the abrasive grains used in the grinding experiments described later.

The test conditions are given in Table 2. Firstly, to investigate the characteristics of the oxides formed, the tests were carried out in a dry environment using the test pieces obtained in the immersion test described in section 2.3. Secondly, to determine the relationship between the test piece oxidation induced by UFBs and the machining of the material and to study its effect on the friction and wear phenomena in actual machining, untreated test pieces were immersed in the evaluation fluids and subjected to the friction and wear tests. After the tests, the wear marks were observed using a digital microscope (VHX-5000, KEYENCE). The area of the wear marks was calculated from the recorded images.

2. 5 Grinding Experiments

In order to verify the validity of the hypothesis about the mechanism behind the UFB effect on the grinding processes studied in the immersion and friction and wear tests, the grinding performance was evaluated in actual machining. The grinding conditions are shown in Table 3. A precision surface grinding machine (EPG-63S, NAGASE INTEGREX) and a WA resinoid grinding wheel (WA100M8B, MITSUI GRINDING WHEEL) were used. The depth of cut and grinding velocity were set at two levels. The combination of a depth of cut of 0.004 mm and a grinding velocity of 83.3 mm/sec. is called the low machining load condition, while the combination of a depth of cut of 0.010 mm and a grinding velocity of 104.2 mm/sec. is called the high machining load condition. These different conditions were set to determine whether the UFB effect varies with the balance between the oxidation rate and the machining speed, based on the estimation that the oxide layer caused by UFBs is considerably thinner than the depth of cut.
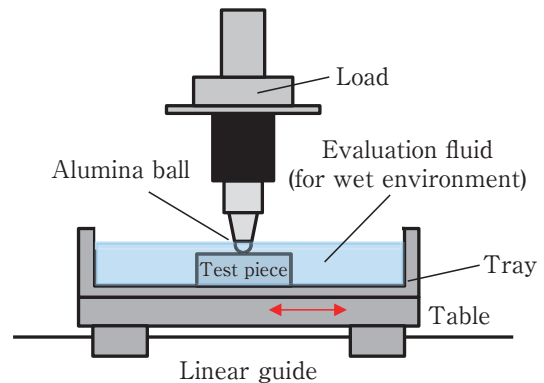

Fig. 2 Experimental system for friction and wear tests

Table 2 Test conditions for friction and wear tests

Test environment	Dry	Wet
Travel	5 mm	
Linear velocity	5 mm/s	
Weight of load	100g	
Test duration	1800s	5400s

Table 3 Grinding conditions

Item		Unit	Low machining load	High machining load
Grinding wheel	Dimensions	[mm]	$\phi 300 \times 30$	
	Peripheral speed	[m/s]	28	
Depth of cut		[mm]	0.004	0.010
Grinding velocity		[mm/s]	83.3	104.2
Removal amount		[mm]	0.8	
Number of grindings		[time]	200	80

Fig. 3 shows an illustration of the measurement of grinding force. A multicomponent dynamometer (9257B, Kistler) was used to measure grinding force. Normal force Fn and tangential force Ft are expressed in Equations (2) and (3) [19]:

$$F_n = C_p \left(\frac{\pi V_W t b}{2 V_G} \right) \tan \alpha \qquad (2)$$

$$F_t = C_p \left(\frac{V_W t b}{V_G} \right) \tan \alpha + \mu F_n \qquad (3)$$

where V_w is the grinding velocity, t is the depth of cut, b is the grinding width, V_G is the peripheral speed of the grinder, μ is the coefficient of friction between the grinder and the workpiece, α is the half-apex angle of the grain, and C_p is the specific grinding energy. The value obtained by dividing F_n by F_t is the ratio of the two force components. A lower ratio of the components indicates higher cutting performance and better grip, while a higher ratio of the components indicates a lower coefficient of friction.

Fig. 4 shows an illustration of grinding ratio measurement. The grinding ratio is calculated by dividing the volume of workpiece removed by the volume of abrasive wear. A higher grinding ratio indicates less abrasive wear. As shown in Fig. 4, when a workpiece narrower than the Grinding wheel
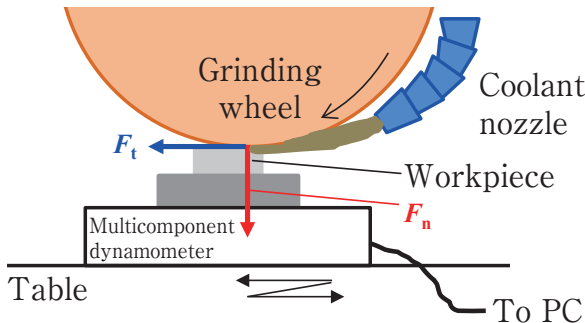
Fig. 3 Grinding force measurement system
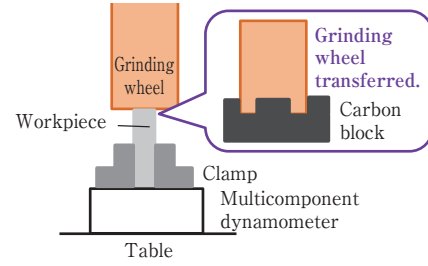
Fig. 4 Grinding ratio measurement system

is ground, the grinding surface of the Grinding wheel has a step. This step was transferred to a carbon block. The profile of the transferred surface was used to measure the step and determine the volume of Grinding wheel wear.

3 Results and Discussion

3.1 Behavior of Test piece Surface Oxidation Induced by UFBs

Table 4 shows pictures of the appearance of the test pieces immersed in the water group (purified water, UFB water) for one day. All of these test pieces have rust on the surface and can be visually identified as oxidized. Focusing on the difference in appearance between the different gases, the test pieces in the purified water and the Air-UFB water show similar changes, but the latter has a slightly larger oxidized area. The test piece in the O_2-UFB water has almost no rust, although slight rust can be seen near the edges. This is probably because O_2-UFBs exist stably in water and are unlikely to collapse [20]. Without a collapse of bubbles, which is the trigger for oxidation, the test piece in O_2UFB was therefore probably not easily oxidized. The unlikelihood of the test piece being oxidized is also due to the high amount of dissolved oxygen in the O_2-UFB water. In an environment with high levels of dissolved oxygen, steel undergoes passivation, resulting in a significantly lower corrosion rate [21]. A measurement of the amount of dissolved oxygen in the O_2-UFB water during preparation showed a maximum of about 38 mg/L. This is about 4.5 times the saturation dissolved oxygen. This means that the high concentration of dissolved oxygen facilitated the passivation of the test piece surface to suppress the corrosion (oxidation) of the material surface.

Table 4 Appearance of test pieces (per water group, after 1-day immersion)

Purified water	Air-UFB water	O_2-UFB water	CO_2-UFB water

In contrast, the test piece in the CO_2-UFB water showed completely different changes than the other gases. While the test piece immersed in the O_2-UFB water partially rusted in red, the test piece immersed in the CO_2-UFB water was completely black. This is due to the likelihood of CO_2-UFBs collapsing [14] to facilitate oxidation of the workpiece, and the acidic solution containing carbonic acid produced when CO_2 was dissolved in water. These changes probably facilitated the oxidation of the test piece surface to produce oxides with a characteristic composition.

Table 5 shows the appearance of the test pieces immersed in the coolant group (coolant diluted with purified water, UFB coolant) for five days. All of these specimens show no visible oxidation. This is probably due to the anticorrosive effect of the coolant itself. Thus, simply immersing the test piece in any coolant and leaving it there will not cause oxidation.
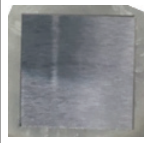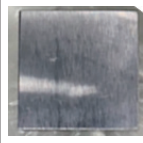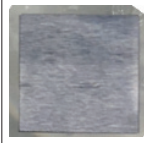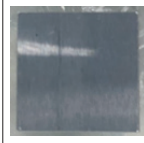
3. 2 Corrosion Rate of test pieces

Fig. 5 shows the results of measuring the corrosion rate of the test pieces oxidized in UFB water. The error bars indicate the maximum and minimum limits of the measurement with N = 3. With respect to the corrosion rate of the test piece in purified water, the test piece in Air-UFB shows 2.4 times, the one in O_2-UFB shows 1.0 times, and the one in CO_2-UFB shows 8.9 times. These results indicate that the presence of UFBs facilitates the oxidation of the test pieces (S50C) used for this study. It should be noted that the test piece in the O_2-UFB water has a corrosion rate almost equal to that of the test piece in purified water, although the former has a smaller oxidized area (Table 4). This is probably because the test piece in the O_2-UFB water is appreciably oxidized in the depth direction, despite the small surface area where oxidation can be visually identified.

3. 3 XPS Analysis of Oxides

Fig. 6 shows the XPS spectrum related to the oxides of the test pieces oxidized in UFB water, and Fig. 7 shows the ratio of the components of the spectrum related to the oxides. In Fig. 6, where the horizontal axis indicates the chemical bonding energy, the graph shows specific values depending on the elements and their chemical bonding state. The "measured" curve is drawn by plotting the raw data obtained by measuring the intensity of the light electrons emitted by the test piece as a function of the bonding energy. The "background" curve represents unnecessary signals due to secondary or scattered electrons. This background data has been subtracted from the measured data and the resulting peaks have been factorized into several model functions and then synthesized. The result is plotted as the "synthesized" curve. In this way, the contribution of each element and its chemical state can be analyzed while reproducing the peak of the measured data [22] [23].

Table 5 Appearance of test pieces (per coolant group, after 5-day immersion)

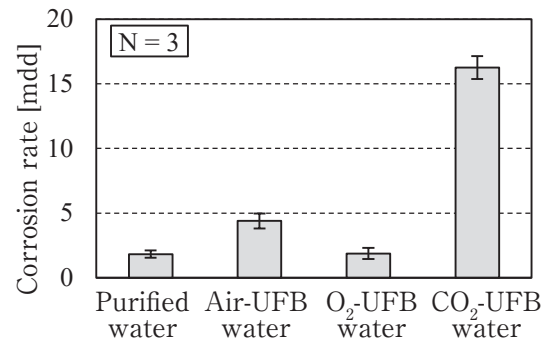| Coolant diluted with purified water	Air-UFB coolant	O_2-UFB coolant	CO_2-UFB coolant

Fig. 5 Corrosion rate of test pieces

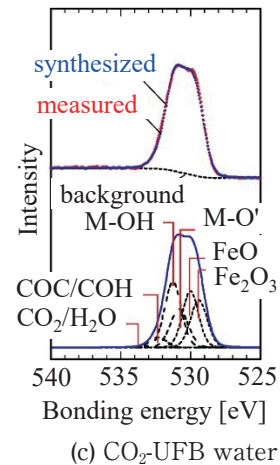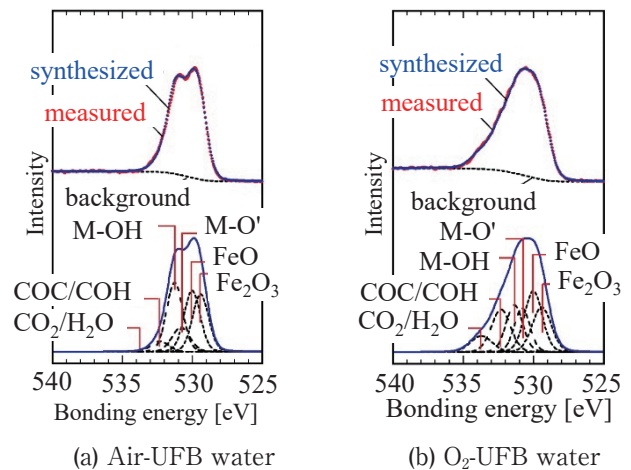(a) Air-UFB water

(b) O_2-UFB water

(c) CO_2-UFB water

Fig. 6 Spectrum related to oxides of oxidized test pieces
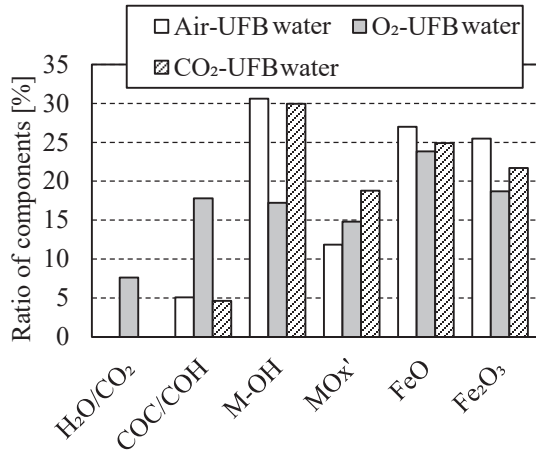
Fig. 7 Ratio of components of the spectrum related to oxides

Fig. 8 Coefficient of friction of oxidized test pieces

Fig. 7 shows that the peak shapes and the composition after separation differ from gas to gas. Specifically, the spectrum for the Air-UFB water increases in the upper right direction with higher proportions of FeO and Fe_2O_3, while the spectrum for the CO_2-UFB water increases in the upper left direction with higher proportions of M-OH' and MOx', which involve high bonding energy. We also examined the Fe 2p spectrum associated with black rust, but did not observe any difference in the spectral profile between different UFB gases. It was verified that the test pieces were oxidized in different visually detectable ways to produce oxides of different compositions depending on the type of UFB gas.

3. 4 Friction Characteristics of Oxides Produced by Various UFBs

The oxides produced in section 3.1 were subjected to the friction and wear tests. The results are shown in Fig. 8. The tests were conducted with N = 3 to 5 for each condition, from which typical data have been plotted in the figure after confirming that the data have little variation. According to the figure, the test pieces oxidized by different UFBs show lower coefficients of friction than the untreated test pieces. The coefficient of friction was highest in the specimen in CO_2-UFB water, almost same level in the test pieces in purified water and Air-UFB water, and lowest in the test pieces in O_2-UFB water. The lowest coefficient of friction in the O_2-UFB water is due to the deep oxidation in the depth direction over a tiny oxidized area which is almost impossible to identify visually (Table 4). Thus, the dry friction and wear tests have shown that the oxides generated in the O_2-UFB water have the lowest coefficient of friction.

3. 5 Friction Characteristics That Simulate Actual Machining

To simulate actual machining, untreated specimens were immersed in the coolant diluted with purified water and various UFB coolants and subjected to the friction and wear tests as they were. The resulting changes in the coefficient of friction are shown in Fig. 9. Similar to section 3.4,
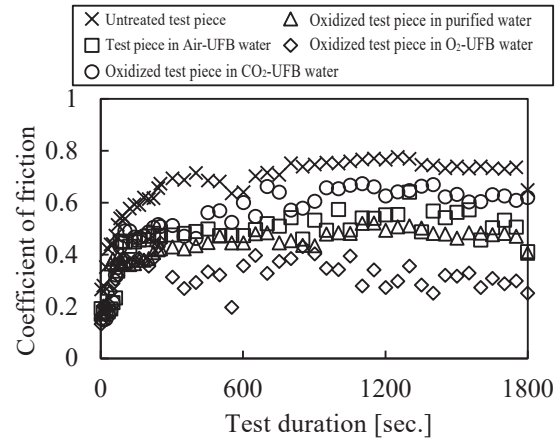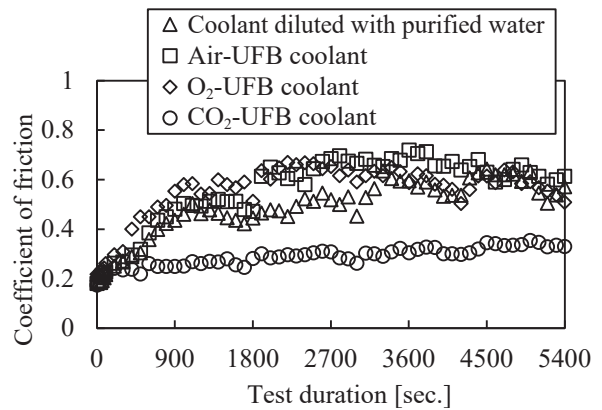

Fig. 9 Coefficient of friction of untreated test pieces

these tests were conducted with N = 3 to 5 for each condition, from which typical data have been plotted in the figure. Although these test pieces were not found to have any visually detectable oxidation when simply immersed and left standing (Table 5), Fig. 9 shows a significant difference in the coefficient of friction between the gas types. In the friction and wear tests on the immersed test pieces, the lowest coefficient of friction was found in the test pieces in CO_2-UFB. The test pieces in O_2-UFB, which had the lowest coefficient of friction in the evaluation of the oxides themselves (Fig. 8), showed a coefficient of friction equivalent to those in Air-UFB in the immersion tests.

Fig. 10 shows an example of wear marks and Fig. 11 shows the results of the wear mark area measurement. The error bars in Fig. 11 indicate the maximum and minimum limits of the measurement with N = 3. A statistical test with a significance level of 5% was performed to find a significant difference in the wear mark area. Thus, in this experimental system, it was confirmed that the wear mark area for the UFB coolant was equal to or slightly larger than that for the coolant diluted with purified water. This is probably because the oxidation induced by UFBs facilitates the removal of material.

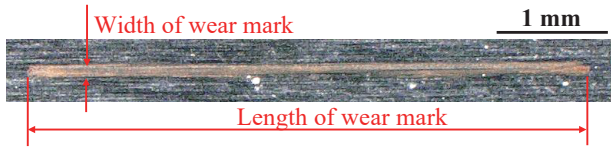Based on the results of section 3.1 and this section, the mechanism behind the UFB effect in
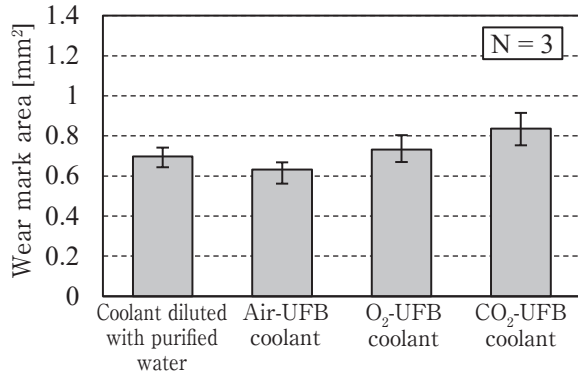
Width of wear mark
1 mm
Length of wear mark

Fig. 10 Example of wear marks (Air-UFB coolant)

N = 3

Wear mark area [mm²]

Coolant diluted with purified water / Air-UFB coolant / O₂-UFB coolant / CO₂-UFB coolant

Fig. 11 Results of wear mark area measurement

UFBs collapse to generate oxidation energy

UFB

Workpiece surface is oxidized.

Workpiece

(a) Collapse of UFBs and oxidation of workpiece surface

Abrasive grains

Surface oxidation and changes in the coefficient of friction

(b) Changes in the coefficient of friction due to oxidized workpiece surface

Fig. 12 Conceptual diagram of the mechanism behind the UFB effect on grinding processes

the coolant is discussed below. As mentioned above, the test pieces that were simply immersed and left in the evaluation fluids of the coolant group did not show any visually detectable changes in appearance, but they did show a significant difference depending on the gas type in the friction and wear tests. This suggests that the UFB effect in the coolant cannot be obtained without some movement, such as mixing, near the machining point. The dynamic stimulus may contribute to the collapse of the UFBs to cause continuous oxidation of the test piece surface, resulting in the changes in friction and wear characteristics.

The above discussion is summarized in Fig. 12. In the vicinity of the machining point, UFBs collapse due to the high-speed rotation of the grinding wheel and other factors. The collapse of UFBs produces OH radicals, which oxidize the workpiece surface to change the surface properties (Fig. 12(a)). In particular, the surface being ground has a high surface energy due to material removal [24] which makes it easily oxidized. Grinding is a phenomenon of friction and wear between the workpiece surface and the abrasive grains. With the collapse of UFBs, the workpiece surface is oxidized to change its friction and wear characteristics, resulting in changes in the grinding performance (Fig. 12(b)).

3. 6 Grinding Performance Using UFB Coolant

This section describes a surface grinding experiment we conducted using O_2-UFB and CO_2-UFB coolants that exhibited the distinctive friction and wear characteristics described in sections 3.4 and 3.5.

Figs. 13 and 14 show the grinding force measurement results and Fig. 15 shows the component ratio calculation results. Machining was carried out with N = 3 for each condition, the average of which is shown in the figures. Under
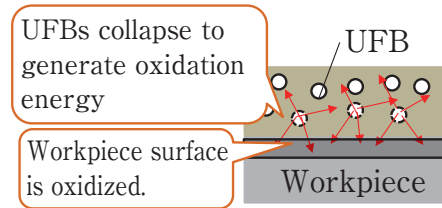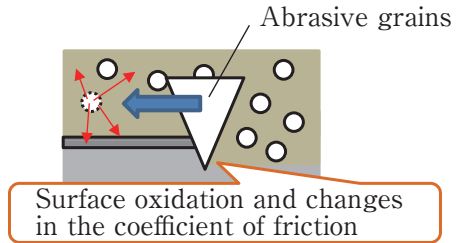
the low machining load condition, the normal force was O_2-UFB > CO_2-UFB > UFB-free and the tangential force was O_2-UFB > UFB-free > CO_2-UFB (Fig. 13). Under the high machining load condition, following the removal of 0.1 mm or larger, the normal force was UFB-free > O_2-UFB > CO_2-UFB and the tangential force was UFB-free > O_2-UFB > CO_2-UFB (Fig. 14). The ratio of the two force components was CO_2-UFB > O_2-UFB ≃ UFB-free for both grinding conditions (Fig. 15), suggesting a decrease in the coefficient of friction between the grinder and the workpiece. These results are consistent with those of the wet friction and wear tests (Fig. 9).

Fig. 16 shows the grinding ratio measurement results. The error bars indicate the maximum and minimum limits of the measurement with N = 3. The grinding ratio under both conditions was improved compared with UFB-free, although the grinding force decreased or increased depending on the gas type. Under the low machining load condition, the grinding ratio for both O_2-UFB and CO_2-UFB was 1.3 times that of UFB-free, with no difference between gas types. However, under the high machining load condition, the grinding ratio for O_2-UFB was 1.2 times and that of CO_2-UFB was 1.7 times, showing the high effect of CO_2-UFB. This is probably due to the difference in the oxides produced. Iron oxide, which is rust formed on the surface of metallic materials, is very hard [25], brittle, and prone to peeling. This means that the workpiece surface oxidized by UFBs is likely to be removed. Oxides produced by O_2-UFBs have a high coefficient of friction, allowing the abrasive grains to grip the workpiece well. The grinder appears to have a very sharp tool, as if it had been dressed for high cutting performance. On the other hand, the oxides produced by CO_2-UFBs have a low coefficient of friction. This suppresses grain wear to improve the grinding ratio.
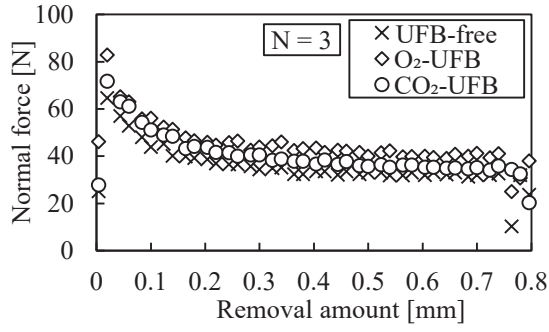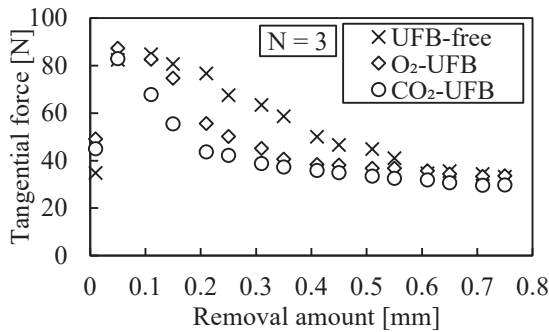
(a) Normal force
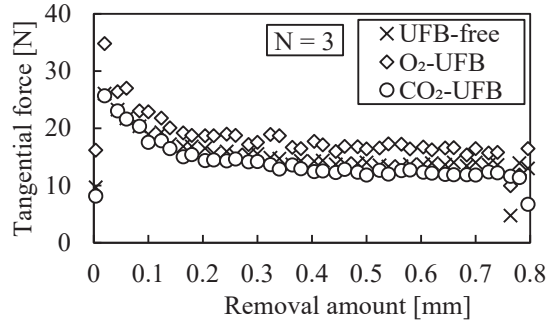
(b) Tangential force

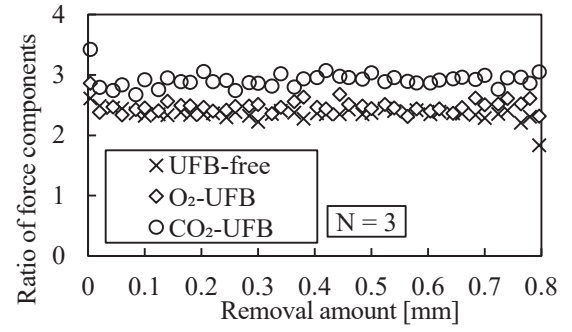**Fig. 13** Results of grinding force measurement (low machining load)
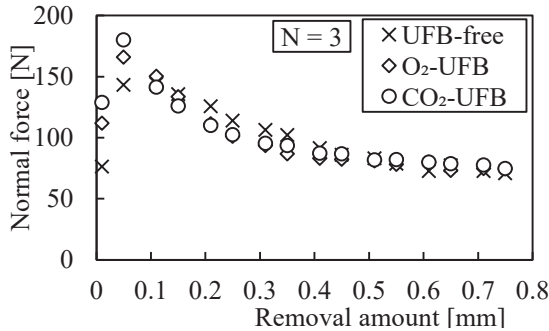

(a) Normal force

(b) Tangential force

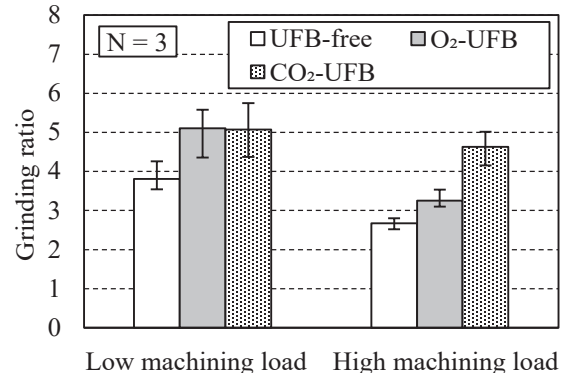**Fig. 14** Results of grinding force measurement (high machining load)

It is discussed below why the test pieces in dry or wet conditions show a high or low coefficient of friction depending on the gas type, resulting in different degrees of improvement in the grinding ratio. This is probably due to the susceptibility of

(a) Low machining load
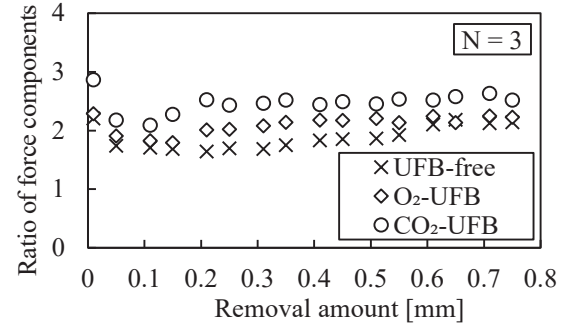
(b) High machining load

Fig. 15 Results of calculation of the ratio of force components

Fig. 16 Results of grinding ratio measurement

UFBs to collapse depending on the gas type. While O_2-UFBs are suitable for test pieces that are oxidized on the surface over a long period of time, such as in immersion testing, CO_2-UFBs are suitable for continuous oxidation of the workpiece surface over a short period of time, such as during grinding. In particular, when the workpiece has a lower coefficient of friction to reduce the tangential grinding force, its material is susceptible to removal, resulting in an improved grinding ratio.

4　Conclusions

In this paper, the mechanism behind the UFB effect on grinding processes using UFB coolant was investigated and discussed by conducting immersion and wear/friction tests, focusing on the oxidation of the workpiece surface induced by the

collapse of UFBs. In addition, grinding experiments were conducted for verification to obtain the following:
⑴ In water, the degree of oxidation of the test piece surface and the composition of the produced oxides depends on the type of UFB gas.
⑵ In coolant, test pieces will not oxidize on the surface simply by being immersed in coolant and left standing. However, adding a dynamic stimulus, such as mixing, changes their friction and wear characteristics.
⑶ The type of gas used in the UFB coolant affects the grinding performance. This change is consistent with the results of the friction and wear tests.
⑷ These tests have shown that the oxidation of the workpiece surface induced by UFBs affects the friction and wear characteristics, leading to changes in grinding performance. This is the mechanism of the UFB effect in grinding processes.

5 Acknowledgement

References
1) ISO 20480-1: 2017. Fine bubble technology - General principles for usage and measurement of fine bubbles- Part 1: Terminology.
2) Kyushu Bureau of Economy, Trade and Industry: "Fine Bubble Application Examples: Fine Bubbles are Transforming Japanese Industry" (2017).
3) IWAI Manabu: "The First Ultra Fine Bubble Coolant," Journal of the Japan Society for Precision Engineering, Vol.87, No.10, pp.809-812 (2021).
4) INAZAWA Katsufumi, EZURA Atsushi, SHINOHARA Naoya, KATO Katsunori, OHMORI Hitoshi, ITOH Nobuhide: "Effect of the Bubble Conditions of the Fine Bubble Coolant on Grinding", Proceedings of 2018 JSPE Autumn Conference, pp.262-263 (2018).
5) INAZAWA Katsufumi, EZURA Atsushi, SHINOHARA Naoya, KATO Katsunori, OHMORI Hitoshi, ITOH Nobuhide: "Effect of Fine Bubble Coolant Using Various Gases on Grinding," Proceedings of 2019 JSPE Autumn Conference, pp.33-34 (2019).
6) KOBAYASHI Hideaki, KAMIJO Yuuki, HIRANO Masahiro, ARAKI Kazunari: "Application of Ultra Fine Bubble Generation Technology to Coolants and Enhancement of Grinding Efficiency," Proceedings of 2020 JSPE Spring Conference, pp.717-718 (2020).
7) WATANABE Takeshi, SUZUKI Hirofumi, TAKADA Ryo, FUKAMI Shingo, MOURI Shigeki, TAKESHITA Tomoharu: "Development of high-accuracy and high-efficiency grinding with ultrafine bubbles coolant, 1st Report: Effects of bubbles on grinding characteristics of cemented carbide," Journal of the Japan Society for Abrasive Technology, Vol.65, No.5, pp.248-253 (2021).
8) WATANABE Takeshi, SUZUKI Hirofumi, TAKADA Ryo, FUKAMI Shingo, MOURI Shigeki, TAKESHITA Tomoharu: "High efficiency grinding with fine bubbles coolant by micropores generator," Journal of the Japan Society for Abrasive Technology, Vol.66, No.9, pp.530-535 (2022).
9) HATAYAMA Yousuke, OKOSHI Hiromu, MORI Terumi, YOSHIDA Futoshi, KURIYAGAWA Tsunemoto, MIZUTANI Masayoshi: "Development of high-concentration ultrafine bubbles generator system for grinding process," Journal of the Japan Society for Abrasive Technology, Vol.67, No.12, pp.657-663 (2023).
10) SERIZAWA Akimi: "Fundamentals of Micro/Nanobubbles," Journal of the Japan Institute of Marine Engineering, Vol.46, No.6, pp.56-61 (2011).
11) TAKAHASHI M., SHIRAI Y., SUGAWA S.: "Free-Radical Generation from Bulk Nanobubbles in Aqueous Electrolyte Solutions: ESR Spin-Trap Observation of Microbubble-Treated Water," Langmuir, 37, pp.5005-5011 (2021).
12) KYB Corporation: Apparatus for producing bubble-containing liquid, method for producing bubble-containing liquid, and system for producing bubble-containing liquid, Patent Number 7033901 (March 11, 2022).
13) ARAKI Kazunari: "Methods and development trends of Fine Bubble Generators," Journal of the Japan Society for Abrasive Technology (JSAT), Vol.66, No.2, pp.79-82 (2022).

14) YAMADA H., KONISHI K., SHIMADA K., MIZUTANI M., KURIYAGAWA T.: "Effect of Ultrafine Bubbles on Pseudomonas Aeruginosa and Staphylococcus Aureus During Sterilization of Machining Fluid," International Journal of Automation Technology, Vol.15, No.1, pp.99-108 (2021).

15) MAEDA Hirotaka: "Method of Measuring Fine Bubble Particle Size Distribution," Journal of the Japan Society for Abrasive Technology (JSAT), Vol.66, No.2, pp.67-70 (2022).

16) IRIE Fumiko: "Particles Tracking Analysis (PTA) for the Size Measurement of Nanoparticles in Liquid," The Association of Powder Process Industry and Engineering, JAPAN, Vol.7, No.7, pp.632-635 (2015).

17) KONISHI Tomohiro: "Introduction of X-ray photoelectron spectroscopy (XPS)," JXTG Technical Review, Vol.60, No.2, pp.58-62 (2018).

18) JIS K 0100-1900 Testing method for corrosivity of industrial water.

19) SHOJI Katsuo: "Grinding Engineering," Yokendo, p.88 (2004).

20) YAMAGUCHI M., MA T., TADAKI D., HIRANO-IWATA A., WATANABE Y., KANETAKA H., FUJIMORI H., TAKEMOTO E., NIWANO M.: "Bactericidal Activity of Bulk Nanobubbles through Active Oxygen Species Generation," Langmuir, 37, pp.9883-9891 (2021).

21) MISAWA Toshihei: "Relation between Metallic Corrosion and Corrosive Environments," Journal of the Japan Society of Colour Material, Vol.54, No.5, pp.309-319 (1981).

22) YOSHIHARA Kazuhiro: "The Basis of AES/XPS/SIMS," Journal of Surface Analysis, Vol.25, No.2, pp.122-135 (2018).

23) TOHMA Hajime: "Background Removal," Journal of Surface Analysis, Vol.8, No.1, pp.49-54 (2001).

24) HASE Alan: "Fundamentals of Tribology," Journal of the Japan Society for Precision Engineering, Vol.81, No.7, pp.643-647 (2015).

25) NANKO Makoto: "Mechanical Properties of Oxidized Scale Generated in Steel Material," FORM TECH REVIEW, No.19, Vol.1, pp.52-55 (2010).

Authors

HATAYAMA Yousuke

Joined the company in 2013. R&D Sect. No.1, Production Technology R&D Center, Engineering Div. Doctor of Engineering. Engaged in research and development related to grinding engineering.

MIZUTANI Masayoshi

Professor, Tohoku University. Green Goals Initiative of Research Center for Green X-Tech and School of Engineering and Graduate School of Biomedical Engineering, Tohoku University.